

MSc Dissertation

Analysis of Integral Operators from Scattering

Problems

Edmund Ridley

August 20, 2006

Acknowledgements

I would like to acknowledge Dr. Marko Lindner and Dr. Stephen Langdon who jointly supervised this project who I am extremely grateful for all the help and knowledge they have given me to enable me to complete this dissertation. Their patience was very much appreciated. All the staff in the mathematics department were also very supportive and helpful, especially those directly involved in the MSc courses, I would like to thank you. My friends and family helped me during this sometimes stressful time over the year, I would like to acknowledge you also.

I would also like to make a special acknowledgement to my late father, who without his support, love and friendship throughout my life I may not have even be doing Mathematics now!

Lastly, I would like to recognise the financial assistance provided by the EPSRC studentship.

Declaration

I confirm this report is all my own work and any material taken from other sources has been fully and properly acknowledged.

Edmund Ridley

Abstract

The classical wave scattering problem is of much interest in many disciplines such as geology and physics. In understanding how solutions behave it is important to study the norms of relevant operators which are connected to the solution. One of these operators defined as A in this project has had little knowledge found about it. How the norm of A behaves as the wavenumber of the incident wave increases is of interest, since this informs us of behaviour when the wave has a high frequency. This project has numerically approximated some relevant norms of part of the operator A which has led to confirmation of results in the literature. These results are presented and discussed in a way that has provided a foundation for future work, enabling perhaps more important results to be found later. The theory and code this project has presented can be easily extended to more general convex smooth shapes.

Contents

1	Introduction	1
2	Background	3
2.1	The Wave Scattering Problem	4
2.2	Literature Results	8
3	A Brief Outline of Norms	9
4	Upper Bounds on $\ S\ _{L^p}$	10
4.1	The Single Layer Potential	11
4.2	The $p = 1$ Norm Single Integral	12
4.3	The $p = \infty$ -norm Single Integral	13
4.4	Double Integral for the One and Infinity Norms	15
4.5	Other Upper Bounds On $\ S\ _{L^p}$ for $p \in (1, \infty)$	19
5	Lower Bounds on $\ S\ _{L^p}$	22
6	Numerical Methods for the Lower and Upper Bounds	23
6.1	Gaussian Quadrature	25
6.1.1	Legendre Polynomial	26
6.2	How Gaussian Quadrature Works in 1-D	26
6.2.1	Example	27
6.2.2	2-D Gaussian Quadrature	28
6.3	Testing the Method	29
6.4	Evaluating the Single Integral	30
7	Speeding Up the Code	32

7.1	<i>For</i> Loops vs Vectors and Matrices	32
7.2	Graded Mesh - The Duffy Transformation	34
7.3	The Duffy Transformation for Piecewise Constants	38
8	Results	39
8.1	1-norm and the ∞ -norm	40
8.2	The 2-norm	44
9	Conclusion	45
10	Future Work	46
10.1	Lower Norms	47
10.2	Further Research into the Two Norm	47
10.3	Looking at the Operator A	48

List of Figures

2.1	Wave Scattering Problem	4
4.1	u Chosen for the One Norm	16
4.2	u Chosen for the Infinity Norm	18
4.3	Upper bound 4.13 for $1 \leq p \leq \infty$ and $k = 1$	21
4.4	Upper bound Using the Riesz-Thorin Interpolation 4.14 for $k = 1$	22
4.5	Combined Upper Bounds from Figures 4.4 and 4.3 for $k = 1$.	23
4.6	Upper Bound using the Symmetric Property for Figure 4.5 .	24
4.7	Symmetric Upper Bound for $k = 1$ Using 4.14 Again	24
7.1	Region Before Transformation	35
7.2	Transformed Triangle 2	36
7.3	The Divided Mesh Used for Triangle 2	37
7.4	Region Before Transformation Using Piecewise Constants . .	39
8.1	Upper Bounds of $\ S\ _{L^p}$ with k increasing for $y(\tau) = (2 \cos \tau, \sin \tau)$	44
8.2	Upper Bounds of $\ S\ _{L^p}$ with k increasing for the Circle . . .	45

List of Tables

4.1	Values of (4.4) for $y(\tau) = (2 \cos \tau + \sin \tau)$	17
4.2	Values of (4.12) for $y(\tau) = (2 \cos \tau, \sin \tau)$	19
5.1	Lower Bound Numeric Approximations for the 2-norm	25
6.1	Single Integral Gaussian Quadrature Code	30
6.2	Double Integral Gaussian Quadrature Code	30
6.3	Approximations of $\ S\ _{L^1} = \ S\ _{L^\infty}$ for a Circle with $t = 0$. .	32
6.4	Approximations of $\ S\ _{L^1} = \ S\ _{L^\infty}$ for Different t for a Circle	33

8.1	Approximation to the 1-norm for the Circle as $k \rightarrow \infty$ using the Single Integral	41
8.2	Results for the 1-Norm as $k \rightarrow \infty$ for $y(\tau) = (2 \cos \tau, \sin \tau)$ using the Single Integral	42
8.3	Approximations for the 2-Norm as $k \rightarrow \infty$ for $y(\tau) = (2 \cos \tau, \sin \tau)$ using the mid-point of the lower and upper bounds	43
8.4	Approximations for the 2-Norm as $k \rightarrow \infty$ for the circle using the mid-point of the lower and upper bounds	43

1 Introduction

There are many different partial differential equations that we come across, of which a small section are on wave scattering. These waves can be acoustic, light, electromagnetic or just vibrations of a drumskin. Knowing how these waves behave, especially when coming in contact with objects is very important. With this knowledge being necessary for solving problems in geology, physics and meteorology to name a few. A use in geology can be investigating the properties such as density and shape of materials that would require significant expense to dig up. Using wave scattering theory the materials can be investigated so that geologists can know where oil, for example, is.

This project has looked at the sound-soft direct wave scattering problem on a convex shape with a smooth boundary (see Background). Looking at the single layer potential S , we gain indications of how the operator A , of which the single layer potential is part, behaves. This then informs us of properties in the error of the problem. The properties that are interesting are how A changes as the wave number k tends to infinity. We look into the properties of A by looking at a part of the operators norm, $\|S\|$. By numerically approximating lower and upper bounds of $\|S\|$ we can plot a region where the norm lies. Conclusions can then be made, with how precise they are depending on the bounds.

In doing this we first need to cover some background material. In Section 2 the classical *wave scattering problem* has been set, with the boundary condition of $u = u^i + u^s = 0$ on the boundary of our convex object with a smooth boundary. We mention the *Helmholtz equation* and its fundamental solution $\phi(x, y)$ which has a singularity at $x = y$. Then using material from [7] and [1] we use *Green's Representation Theorem* to establish our key integral equation (2.7), which we state here as $A\phi = f$. Performing some

manipulation of the operator A using theory from projection methods in [9] we state why the norms of $\|A\|$ and $\|A^{-1}\|$ are crucial in finding out about the behaviour of the error in the solution (i.e. $\|\phi - \phi_n\|$).

This project looks at the single layer potential (2.8), which is a key part of the operator A , and is an important first step into looking at the operator A as a whole. The choice of investigating A instead of A^{-1} is that much work has been done on the inverse operator such as in the paper [1], and less is known about A . In looking at the operator S , we analyse $\|S\|$ in L^p space (i.e. $\|S\|_{L^p}$). We establish upper (Section 4) and lower bounds (Section 5) on $\|S\|_{L^p}$. We start by looking at two special cases where $p = 1$ and $p = \infty$ as these provide us with upper bounds on $\|S\|_{L^p}$ for $1 < p < \infty$. These two cases fortunately have explicit formulae for $\|S\|_{L^p}$, unlike for $p = 2$. The explicit formulae are also single integrals, whereas for the 2-norm we are required to compute a double integral. Although, we also discuss how it is possible to use the more complicated double integrals for the 1-norm and ∞ -norm to approximate $\|S\|_{L^p}$. After this we discuss two upper bounds, one of which is found by manipulation of $\|S\|_{L^p}$ and another which is found by use of the *Riesz-Thorin interpolation* formula. With these upper bounds, and other arguments that give us $\|S\|_{L^p}$ being symmetric about $p = 2$ and also $p = 2$ being a global minimum, we are able to combine these upper bounds to provide us with the figures towards the end of Section 4..

The next stage is to look at the lower bounds of $\|S\|_{L^p}$, which is done in Section 5. In particular in this section we look at $\|S\|_{L^2}$, for the reason that it is then possible to make direct comparisons with results from [3] and [1]. These results being on various shapes, such as a circles and convex objects with a smooth boundary (both of which are looked at here) in [3] and polyhedra in [1]. In looking at the lower bound for $\|S\|_{L^2}$, we numerically

compute $\frac{\|Su\|_{L^2}}{\|u\|_{L^2}}$, where we seek to find a u such as our numerical approximation gives a value close to the real value of $\|S\|_{L^2}$. This lower bound can then be combined with the upper bound to provide us with the figures in Section 8 and Section 9.

In Section 6 we then talk about the numerical methods used to compute these upper and lower bounds. Gaussian quadrature is introduced here, and an example is used to give an idea into how it works. Also, we include some equations which test the method (and the code) to indicate how Gaussian quadrature converges with n (the number of Gaussian quadrature points) going to infinity. With Section 7 continuing this numerics by discussing how it is possible to speed up the code in MATLAB with the use of vectors and matrices. Then we go on to discuss one way to use the quadrature points more effectively by use of a graded mesh, with at the same time taking consideration of the singularity.

Next we have Section 8 on the results that have been obtained. With a table showing how our numerically approximated $\|S\|_{L^2}$ changes as $k \rightarrow \infty$. Also here we include figures of the lower and upper bounds as k increases. Then we go on to our conclusions and relate then to literature, and finally future work which would be the next stages if more time was available.

2 Background

There is much theory on wave scattering, and hence here is a condensed and brief outline of the general problem for the *direct scattering problem*. That is, the problem of finding the *scattered field* after a wave has hit an object, when the *incident wave* is known.

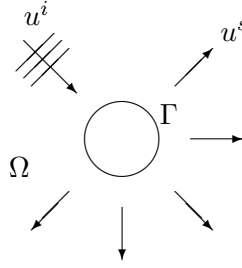


Figure 2.1: Wave Scattering Problem

2.1 The Wave Scattering Problem

This project is looking at the 2D wave scattering problem (see Figure 2.1). We have an incident wave u^i hitting the object which has boundary Γ . Then the wave is scattered, and we have the scattered field u^s in our region Ω , with Ω being the exterior to the domain. The condition on the boundary chosen for this project is that $u := u^i + u^s = 0$ on Γ (this Dirichlet condition is referred to as sound-soft, with a Neumann condition referring to sound-hard). The u^i is known and the u^s is to be found, and we then have the *Helmholtz equation*,

$$\nabla^2 u + k^2 u = 0, \quad (2.1)$$

where k is the wavenumber. The wavenumber is related to the frequency by,

$$k = \frac{w}{c}$$

with w being the frequency of the incident wave and c is the speed of sound. The Helmholtz equation is satisfied by u^i , u^s and $u = u^i + u^s$. The fundamental solution for the 2D problem is

$$\phi(x, y) = \frac{i}{4} H_0^1(k|x - y|), \quad (2.2)$$

where H_0^1 is a Hankel function of the first kind and is defined by

$$H_R^1(x) = J_R(x) + iY_R(x)$$

with $J_R(x)$ being a Bessel function of the first kind and $Y_R(x)$ being a Bessel function of the second kind (also known as the Neumann function). These Bessel functions originate from being solutions of a special case of the Sturm-Liouville Boundary Value Problem,

$$x^2 y'' + xy' + (x^2 - R^2)y = 0.$$

We will not investigate the Hankel function further, instead we will note two important features.

- $H_0^1(k|x-y|)$ has a logarithmic singularity at $x = y$
- H_0^1 is symmetric about the origin, i.e. $H_0^1(k|x-y|) = H_0^1(k|y-x|)$.

More can be found about Hankel functions in [2] and [4].

We can then take *Green's Representation Theorem* from [1],

$$u(x) = u^i(x) - \int_{\Gamma} \phi(x, y) \frac{\partial u(y)}{\partial n} ds(y), \quad x \in \Omega, \quad (2.3)$$

where $\frac{\partial u}{\partial n}$ is the normal derivative. Then on the boundary (where $u(x) = 0$) this becomes,

$$\begin{aligned} 0 &= u^i(x) - \int_{\Gamma} \phi(x, y) \frac{\partial u(y)}{\partial n} ds(y), \quad x \in \Gamma \\ \Rightarrow u^i(x) &= \int_{\Gamma} \phi(x, y) \frac{\partial u(y)}{\partial n} ds(y), \quad x \in \Gamma. \end{aligned} \quad (2.4)$$

This is a first kind integral equation for the unknown boundary data $\frac{\partial u}{\partial n}$. However, for some values of k there is not a unique solution. By taking the normal derivative and letting $x \rightarrow \Gamma$ we have

$$\frac{1}{2} \frac{\partial u(x)}{\partial n} = \frac{\partial u^i(x)}{\partial n} - \int_{\Gamma} \frac{\partial \phi(x, y)}{\partial n(x)} \frac{\partial u(y)}{\partial n} ds(y) \quad (2.5)$$

This is because of a jump condition as we approach the boundary, meaning

$$\int_{\Gamma} \frac{\partial \phi(x, y)}{\partial n(x)} \frac{\partial u(y)}{\partial n} ds(y), \quad x \in \Omega$$

becomes

$$\int_{\Gamma} \frac{\partial \phi(x, y)}{\partial n(x)} \frac{\partial u(y)}{\partial n} ds(y) - \frac{\partial u(x)}{\partial n}, \quad x \in \Gamma$$

(see [8] and [7]). By multiplying (2.4) by $i\eta$ and adding (2.5), then multiplying all through by 2 we get,

$$\frac{\partial u(x)}{\partial n} + 2 \int_{\Gamma} \left\{ \frac{\partial \phi(x, y)}{\partial n} + i\eta \phi(x, y) \right\} \frac{\partial u(y)}{\partial n} ds(y) = f(x), \quad x \in \Gamma, \quad (2.6)$$

where $f(x) = 2 \left(\frac{\partial u^i}{\partial n} + i\eta u^i(x) \right)$. Thus we have our unknown

$$\frac{\partial u}{\partial n}$$

and the following integral equation,

$$(I - B) \frac{\partial u}{\partial n} = f. \quad (2.7)$$

Then denoting

$$Bv = \int_{\Gamma} R_k \cdot v$$

where

$$R_k = 2 \left[\frac{\partial \phi(x, y)}{\partial n(x)} + i\eta \phi(x, y) \right].$$

This integral can then be split into the single-layer (2.8) and double-layer (2.9) potentials (taken from [7]),

$$Su := \int_{\Gamma} u(y) \phi(x, y) ds(y), \quad x \in \Gamma \quad (2.8)$$

$$Du := \int_{\Gamma} u(y) \frac{\partial \phi(x, y)}{\partial n(y)} ds(y), \quad x \in \Gamma. \quad (2.9)$$

Denoting the double layer potential as D and the single layer potential as S we have the operator,

$$A = I + 2D + 2i\eta S.$$

Thus, summarising the background so far we have the equation,

$$A\phi = f \quad (2.10)$$

to solve, where $A = I + 2(D + i\eta S) = I - B$, and we seek the solution ϕ . To solve (2.1) numerically one can use a projection method, such as the Galerkin and collocation methods. Writing the problem as $A\phi = (I - B)\phi = f$ then we can look at how projection methods can be used to look at the error analysis of this problem. From Section 3 in [9] there is much description on precisely how the projection methods can be used to look at the error analysis. We will take the key outline of the argument relevant for the problem that has been looked at in this project.

We have a projection operator P_n which when applied to (2.10) we have,

$$P_n A \phi_n = P_n f$$

and hence

$$P_n(I - B)\phi_n = P_n f \text{ (equation (3.1.24) in [9])}.$$

Noting that $P_n \phi_n = \phi_n$, we can then write,

$$(I - P_n B)\phi_n = P_n f \text{ (equation (3.1.25) in [9])},$$

where the $A_n = (I - P_n B)$. A_n is determined by the method. Therefore we now have,

$$A_n \phi_n = P_n f, \text{ i.e. } \phi_n = A_n^{-1} P_n f.$$

We are interested in ϕ_n since this is our approximation to the solution ϕ , and thus knowledge of A_n^{-1} is also of interest. Using equation (3.1.27) from [9] we can write that,

$$A_n = A[I + A^{-1}(B - P_n B)].$$

Then using Theorem 3.1.1 in [9] and assuming that $\|B - P_n B\| \rightarrow 0$ as $n \rightarrow \infty$ we can say that A_n^{-1} exists and is also bounded (i.e. $\|A_n^{-1}\| < \infty$ for sufficiently large n). Information about the operators A and A^{-1} can tell

us about A_n and A_n^{-1} , and hence tell us something about how ϕ_n depends on k . For our particular problem we can use the Theorem 3.1.1, and the equations (3.1.30) and (3.1.31) to say that,

$$\frac{1}{\|A_n\|} \|\phi - P_n\phi\| \leq \|\phi - \phi_n\| \leq \|A_n^{-1}\| \|\phi - P_n\phi\|.$$

This gives us upper and lower bounds for the error term norm, $\|\phi - \phi_n\|$. In this project we are concentrating on a part of the operator A . We are looking at the operator S , our single layer potential. Using this is the first step in investigating the norm of A , $\|A\|$. Much work has been done on the inverse in such papers as [3] and [1]. Information on $\|A\|$ is not so vast, with this project giving a first stage on how to tackle $\|A\|$. Also, of great interest is to know the condition number of A ,

$$\text{cond } A := \|A\| \cdot \|A^{-1}\|.$$

The condition number indicates how much a change in f effects the approximate solution ϕ_n . A large condition number represents a large change, and hence a small amount of error in f creates a big error in the solution. Clearly, knowledge of $\|A\|$ helps to understand the condition number.

2.2 Literature Results

In [3] we have the two dimensional results that

$$\|A\|_2 \leq \mathcal{O}(k^{\frac{1}{3}}) \text{ as } k \rightarrow \infty,$$

for a circle and

$$\|A\|_2 \leq \mathcal{O}(k^{\frac{1}{2}}) \text{ as } k \rightarrow \infty$$

for a general convex obstacle with smooth boundary (here the 2-norm has been looked at, indicated by the subscript 2 on the norm of A). However,

much of the results gathered have been on $\|A^{-1}\|$. These results include $\|A^{-1}\| \leq 2$ (for sufficiently large k) for a circle shown in [3] and an upper bound for $\|A^{-1}\|$ for polyhedra in [1].

3 A Brief Outline of Norms

A set X with an operation $+$ is a *linear space* if $x + y \in X$, $\alpha x \in X \forall \alpha \in \mathbb{C}, \forall x, y \in X$ and the following axioms hold:

- $x + y = y + x$
- $(x + y) + z = x + (y + z)$
- $\exists 0 \in X$ such that $0 + x = x \forall x \in X$
- $\forall x \in X \exists "-x" \in X$ such that $x + (-x) = 0$
- $(\alpha + \beta)x = \alpha x + \beta x$
- $\alpha(x + y) = \alpha x + \alpha y$
- $1 \cdot x = x, \forall x \in X$

If X, Y are linear spaces and $A : X \rightarrow Y$ is a map with,

- $A(x + y) = Ax + Ay, \forall x, y \in X$
- $A(\alpha x) = \alpha \cdot Ax, : \forall \alpha \in \mathbb{C}, x \in X$

then we call A a *linear operator* from X to Y .

A linear space X is called a *normed linear space* if there is a map $\|\cdot\| : X \rightarrow \mathbb{R}_+$ such that

- $\|x\| \geq 0, \forall x \in X$ with $\|x\| = 0 \iff x = 0$
- $\|\alpha x\| = |\alpha| \cdot \|x\|, \forall \alpha \in \mathbb{C}, x \in X$

- $\|x + y\| \leq \|x\| + \|y\|, \forall x, y \in X.$

Examples of some linear spaces with norms are

1. $X = \mathbb{R}^n$ with $\|(x_1, \dots, x_n)\| = \sqrt[p]{|x_1|^p + \dots + |x_n|^p}$ where $p \in [1, \infty).$

- For $p = 2$, we have the Euclid Norm $\|(x_1, x_2)\| = \sqrt{|x_1|^2 + |x_2|^2}$

2. $X = \mathbb{R}^n$ with

$$\begin{aligned} \|(x_1, \dots, x_n)\| &= \max\{|x_1|, \dots, |x_n|\} \\ &= \lim_{p \rightarrow \infty} \sqrt[p]{|x_1|^p + \dots + |x_n|^p} \end{aligned}$$

3. $X = L^p[0, 1]$ with $\|f\| = \sqrt[p]{\int_0^1 |f(t)|^p dt}$

- Note: $L^p[0, 1]$ is the space such that $\int_0^1 |f(x)|^p dx$ exists and is finite.

For our problem the $L^p[0, 2\pi]$ norm will be looked at, especially $L^1[0, 2\pi]$, $L^\infty[0, 2\pi]$ and $L^2[0, 2\pi]$, with $\|f\| = \sup\{|f(t)| : t \in [0, 2\pi]\}$ in $L^\infty[0, 2\pi]$.

Finally, we say that $A : X \rightarrow Y$ is *bounded* if $\exists C > 0$ such that,

$$\|Ax\| \leq C, \forall x \text{ with } \|x\| = 1$$

$$\text{i.e. } \|Ax\| \leq C\|x\|, \forall x \in X \quad (3.1)$$

where the smallest C is called the norm of A written $\|A\|$.

4 Upper Bounds on $\|S\|_{L^p}$

In investigating $\|S\|_{L^2}$ (referred to as the 2-norm) an upper bound and a lower bound are required, with the accuracy of the 2-norm dependent on how good these bounds are. An upper bound can be found by using the values of the 1-norm ($\|S\|_{L^1}$) and the ∞ -norm ($\|S\|_{L^\infty}$). Also, by manipulating (4.4) it is possible to find upper bounds on all p .

4.1 The Single Layer Potential

This project will be concentrating on the single layer potential operator,

$$(Su)(x) = \int_{\Gamma} H_0^1(k|x-y|)u(y)ds(y) \quad (4.1)$$

where Γ is a general convex shape with smooth boundaries that describes the object. This can be re-written

$$(Su)(x) = \int_{\Gamma} \tilde{\kappa}(x,y)u(y)ds(y)$$

with $\tilde{\kappa}(x,y) = H_0^1(k|x-y|)$. The p -norm of the single layer potential is therefore

$$\begin{aligned} \|Su\|_{L^p(\Gamma)} &= \left(\int_{\Gamma} |(Su)(x)|^p ds(x) \right)^{\frac{1}{p}} \\ &= \left(\int_{\Gamma} \left| \int_{\Gamma} \tilde{\kappa}(x,y)u(y)ds(y) \right|^p ds(x) \right)^{\frac{1}{p}} \end{aligned} \quad (4.2)$$

Parameterising Γ by a function $y(\tau)$ over the interval $[0, 2\pi]$ gives

$$\begin{aligned} (Su)(x) &= \int_{\Gamma} H_0^1(k|x-y|)u(y)ds(y) \\ &= \int_0^{2\pi} \frac{i}{4} H_0^1(k|y(t) - y(\tau)|)u(y(\tau))|y'(\tau)|d\tau \end{aligned}$$

with $ds(y(\tau)) = |y'(\tau)|d\tau$. Hence giving us a new equivalent parameterised p -norm of the single layer potential of

$$\|Su\|_{L^p(\Gamma)} = \left(\int_0^{2\pi} \left| \int_0^{2\pi} \kappa(t,\tau)u(\tau)|y'(\tau)|d\tau \right|^p |y'(t)|dt \right)^{\frac{1}{p}}. \quad (4.3)$$

Recall that $\|S\|$ is the smallest $M \geq 0$ (using equation (3.1)) such that

$$\frac{\|Su\|}{\|u\|} \leq M, \forall u \neq 0$$

or equivalently

$$\|S\| = \sup_{u \neq 0} \frac{\|Su\|}{\|u\|}.$$

If $\|u\| = 1$ we have

$$\|S\| = \sup_{\|u\|=1} \|Su\|$$

hence

$$\begin{aligned} \|S\|_{L^p(\Gamma)} &= \sup_{\|u\|_{L^p}=1} \|Su\| \\ &= \sup_{\|u\|_{L^p}=1} \left(\int_0^{2\pi} \left| \int_0^{2\pi} \kappa(t, \tau) u(\tau) |y'(\tau)| d\tau \right|^p |y'(t)| dt \right)^{\frac{1}{p}} \end{aligned} \quad (4.4)$$

For two special cases where $p = 1$ and $p = \infty$ this equation can be transformed into a single integral.

4.2 The $p = 1$ Norm Single Integral

Taking equation (4.2) we can perform some manipulations on this to put it into the form

$$\|Su\|_{L^1} \leq M_1 \|u\|_{L^1}.$$

Letting $p = 1$ (4.2) gives

$$\begin{aligned} \|Su\|_{L^1(\Gamma)} &= \int_{\Gamma} \left| \int_{\Gamma} \kappa(x, y) u(y) ds(y) \right| ds(x) \\ &\leq \int_{\Gamma} \left(\int_{\Gamma} |\kappa(x, y)| |u(y)| ds(y) \right) ds(x). \end{aligned} \quad (4.5)$$

Then swapping the integration,

$$\|Su\|_{L^1(\Gamma)} = \int_{\Gamma} \left(\int_{\Gamma} |\kappa(x, y)| |u(y)| ds(x) \right) ds(y)$$

and taking the $|u(y)|$ out since it is independent of x

$$\|Su\|_{L^1(\Gamma)} = \int_{\Gamma} \left(\int_{\Gamma} |\kappa(x, y)| ds(x) \right) |u(y)| ds(y)$$

Then parameterising this gives,

$$\begin{aligned} \|Su\|_{L^1(\Gamma)} &= \int_0^{2\pi} \left(\int_0^{2\pi} |\kappa(t, \tau)| |y'(t)| dt \right) |u(\tau)| |y'(\tau)| d\tau \\ &\leq \left(\sup_{\tau \in [0, 2\pi]} \int_0^{2\pi} |\kappa(t, \tau)| |y'(t)| dt \right) \int_0^{2\pi} |u(\tau)| |y'(\tau)| d\tau \\ &= M_1 \|u\|_{L^1[0, 2\pi]}, \end{aligned}$$

where

$$M_1 := \sup_{\tau \in [0, 2\pi]} \int_0^{2\pi} |\kappa(t, \tau)| |y'(t)| dt.$$

We can choose appropriate functions (as shown in section(4.4)) so that this M_1 is the smallest $M_1 \geq 0$ and hence we can write,

$$\|S\|_{L^1(\Gamma)} = \sup_{\tau \in [0, 2\pi]} \int_0^{2\pi} |\kappa(t, \tau)| |y'(t)| dt. \quad (4.6)$$

The advantage of (4.6) compared to (4.4) is not only that it is a single integral and thus less costly to numerically compute, but more importantly there is no u term. This means it is not needed to look for a u , as is required when computing (4.4).

(Results computed using (4.6) can be seen in Table 8.1 and Table 8.2).

4.3 The $p = \infty$ -norm Single Integral

As with the one norm we can perform some manipulations on (4.2) to obtain

$$\|Su\|_{L^\infty[0, 2\pi]} \leq M_\infty \|u\|_{L^\infty[0, 2\pi]}.$$

We have

$$\begin{aligned} \|Su\|_{L^\infty(\Gamma)} &= \sup_{x \in \Gamma} |(Su)(x)| \\ &= \sup_{x \in \Gamma} \left| \int_{\Gamma} \kappa(x, y) u(y) ds(y) \right| \\ &\leq \sup_{x \in \Gamma} \int_{\Gamma} |\kappa(x, y)| |u(y)| ds(y) \end{aligned}$$

Taking the supremum of $|u(y)|$, it can then be taken out of the integral such that,

$$\|Su\|_{L^\infty(\Gamma)} \leq \left(\sup_{x \in \Gamma} \int_{\Gamma} |\kappa(x, y)| ds(y) \right) \left(\sup_{y \in \Gamma} |u(y)| \right)$$

Then parameterising we have,

$$\|Su\|_{L^\infty[0, 2\pi]} = \left(\sup_{t \in [0, 2\pi]} \int_0^{2\pi} |\kappa(t, \tau)| |y'(\tau)| d\tau \right) \left(\sup_{\tau \in [0, 2\pi]} |u(\tau)| \right)$$

and hence as required,

$$\|Su\|_{L^\infty(\Gamma)} = M_\infty \|u\|_{L^\infty(\Gamma)}$$

where

$$M_\infty := \sup_{t \in [0, 2\pi]} \int_0^{2\pi} |\kappa(t, \tau)| |y'(\tau)| d\tau.$$

This can be shown to be the smallest $M_\infty \geq 0$ (as shown in Section(4.4)) and therefore we have,

$$\|S\|_{L^\infty(\Gamma)} = \sup_{t \in [0, 2\pi]} \int_0^{2\pi} |\kappa(t, \tau)| |y'(\tau)| d\tau. \quad (4.7)$$

As with the single integral for the one norm, this gives us the same advantages. In fact, because of the symmetry of the Hankel function we have that,

$$\begin{aligned} \|S\|_{L^1(\Gamma)} &= \sup_{y \in \Gamma} \int_{\Gamma} \left| \frac{i}{4} H_0^1(k|x-y|) \right| ds(x) \\ &= \sup_{y \in \Gamma} \int_{\Gamma} \left| \frac{i}{4} H_0^1(k|y-x|) \right| ds(x) \\ &= \sup_{x \in \Gamma} \int_{\Gamma} \left| \frac{i}{4} H_0^1(k|x-y|) \right| ds(y) \\ &= \|S\|_{L^\infty(\Gamma)}, \end{aligned}$$

so $M_1 = M_\infty$. More generally we have the result

$$\|S\|_{L^p} = \|S\|_{L^q}, \text{ if } \frac{1}{p} + \frac{1}{q} = 1 \quad (4.8)$$

for all $p \in [1, \infty]$. This means that $\|S\|_{L^p}$ is symmetric about $p = 2$ (in the sense that $p = 2$ is the mid-point of the interval $[1, \infty]$), which will be used later on.

4.4 Double Integral for the One and Infinity Norms

Although we have the single integrals for the 1-norm and the ∞ -norm, (4.6) and (4.7) respectively, it is also possible to compute them accurately using the double integral (4.4). Simplifying this as a matrix problem we have,

$$Su = \begin{pmatrix} \leftarrow & \tau & \rightarrow \\ \uparrow & & \\ t & & K \\ \downarrow & & \end{pmatrix} \begin{pmatrix} \\ \\ u \\ \end{pmatrix},$$

where $K = \kappa(t, \tau)|y'(\tau)|$. The 1-norm corresponds to the maximum column sum and the ∞ -norm corresponds to the maximum row sum of K .

Equation (4.4) for $p = 1$ is

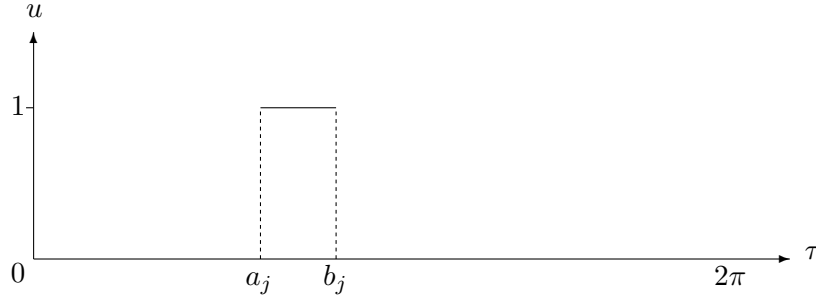
$$\|S\|_{L^1(\Gamma)} = \sup_{\|u\|_{L^1}=1} \int_0^{2\pi} \left| \int_0^{2\pi} \kappa(t, \tau)u(\tau)|y'(\tau)|d\tau \right| |y'(t)|dt \quad (4.9)$$

With the 1-norm being equivalent to a column sum, we need to find the value of τ say τ^* where this is greatest. Thus, by choosing u such that it ‘picks’ out this column it would give an approximation for the supremum of the 1-norm. Looking at Figure 4.1 we have a piecewise constant over the interval $[a_j, b_j]$ where $a_j = \frac{2\pi(j-1)}{N}$ and $b_j = \frac{2\pi j}{N}$, and zero elsewhere. The value of this piecewise constant is required to be chosen such that

$$\begin{aligned} \|u\|_{L^1(\Gamma)} &= \int_{\Gamma} |u(y)|ds(y) \\ &= \int_0^{2\pi} |u(y(\tau))||y'(\tau)|d\tau \\ &= 1. \end{aligned}$$

Choosing $u = 1$ over the interval $[a_j, b_j]$ and zero everywhere else this becomes,

$$\|u\|_{L^1} = \int_{a_j}^{b_j} |y'(\tau)|d\tau. \quad (4.10)$$

Figure 4.1: u Chosen for the One Norm

Thus, to keep $\|u\|_{L^1} = 1$ we are required to divide by $\int_{a_j}^{b_j} |y'(\tau)| d\tau$. Trying N different u with just one piecewise constant where $u = 1$ over the interval $[a_j, b_j]$ for $j = 1, \dots, N$, and $u = 0$ over the rest of the interval (i.e. $[0, a_j]$ and $[b_j, 2\pi]$). For each u ,

$$\int_0^{2\pi} \left| \int_0^{2\pi} \kappa(t, \tau) u(\tau) |y'(\tau)| d\tau \right| |y'(t)| dt.$$

needs to be divided by

$$\int_{a_j}^{b_j} |y'(\tau)| d\tau.$$

We then take the largest value and this is the approximation for $\|S\|_{L^1}$. Then as N is increased the approximation improves.

Table 4.1 shows that as N (which concentrates u on a smaller and smaller part of $K(t, \tau)$) increases the values given by the double integral become closer to the single integral value (in Table 8.2).

With the ∞ -norm being the maximum row sum, it is required to find a u such that

$$\|u\|_{L^\infty(\Gamma)} = \sup_{\tau \in [0, 2\pi]} |u(\tau)| = 1 \quad (4.11)$$

and which ‘picks’ out the maximum row sum. The maximum row sum can be found in this case by using the single integral. This is used by choosing

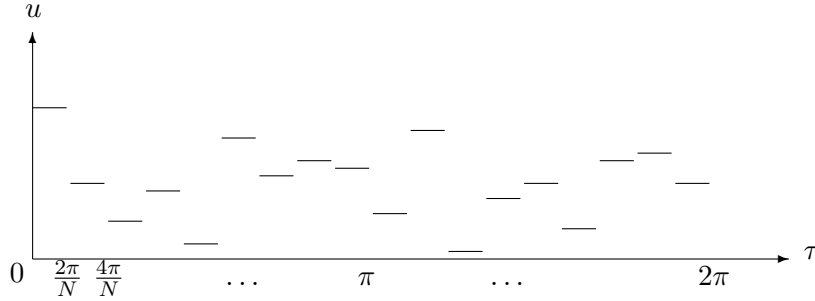
No. of Piecewise Constants	$k = 1$	$k = 2$
1	0.8324275994	0.23012335522458
2	1.0414252323	0.49073840309276
4	1.4298599218	0.71693171534810
8	1.5807037799	1.09042637401177
16	1.6554936274	1.15937045669100
32	1.6839774230	1.21630454860917
64	1.6925392013	1.23577686095915
128	1.6950365160	1.24129630635884
256	1.6957527179	1.24283441218079

Table 4.1: Values of (4.4) for $y(\tau) = (2 \cos \tau + \sin \tau)$

many t , and remembering the value of t say t^* where the single integral is largest. This value of t^* indicates the row which has the maximum sum. Choosing a u which then multiplies each entry in such a way that this is maximised would give the required u to find $\|u\|_{L^\infty(\Gamma)}$. Hence, since it is only necessary for the supremum of the $|u|$ to be one it is possible to let all $|u| = 1$. Splitting u into piecewise constants, and choosing the piecewise constants such that they return the maximum real positive value. This means each $K(t^*, \tau)$ needs to be multiplied by

$$U_j = \frac{|K(t^*, \tau)|}{K(t^*, \tau)},$$

where the U_j is the j th piecewise constant, where $j = 1, \dots, N$ as with the 1-norm. Therefore, in this case the real and imaginary part of u would look

Figure 4.2: u Chosen for the Infinity Norm

something like Figure 4.2. $\|Su\|_{L^\infty}$ can then be found since,

$$\begin{aligned} \|Su\|_{L^\infty} &= \max_{x \in \Gamma} |(Su)(x)| \\ &\approx \max_{t \in [0, 2\pi]} \left| \sum_{j=1}^N \frac{|K(t^*, \tau_j)|}{K(t^*, \tau_j)} \int_{a_j}^{b_j} K(t, \tau_j) d\tau \right| \end{aligned} \quad (4.12)$$

Since

$$u = \sum_{j=1}^N U_j \chi_j$$

where $U_j = \frac{|K(t^*, \tau_j)|}{K(t^*, \tau_j)}$ and χ_j is the characteristic function of the interval $[a_j, b_j]$. Then we have $\|u\|_{L^\infty} = 1$ in the interval $[0, 2\pi]$. Thus,

$$\max_{t \in [0, 2\pi]} \left| \sum_{j=1}^N \frac{|K(t^*, \tau_j)|}{K(t^*, \tau_j)} \int_{a_j}^{b_j} K(t, \tau_j) d\tau \right| \approx \|S\|_{L^\infty}$$

with the approximation improving as N increases.

Table 4.2 shows that as N (the number of piecewise constants) increases the values given by the double integral become closer to the single integral value. All the values have been taken using a large n Gaussian Quadrature points, and are converging.

Number of Piecewise Constants	$k = 1$	$k = 2$
1	1.02268644630414	0.36106346459050
2	1.31546183059806	0.58603913271996
4	1.49238353781992	0.81049822013627
8	1.62799322382511	1.09309495375556
16	1.66182296004815	1.17544163253251
32	1.68166215056378	1.22204280535008
64	1.68608506923276	1.23270470271323
128	1.68792226061701	1.23673616359326
256	1.68834810758787	1.23767714177830
512	1.68852172630963	1.23802042310760

Table 4.2: Values of (4.12) for $y(\tau) = (2 \cos \tau, \sin \tau)$

4.5 Other Upper Bounds On $\|S\|_{L^p}$ for $p \in (1, \infty)$

The $p = 2$ norm has the most interest and it would be good to see how the $\|S\|_{L^2}$ changes as $k \rightarrow \infty$. Equation (4.4) can provide a lower bound for the two norm, and as more u are chosen the bound should improve. However, an upper bound is also needed. With some manipulation an upper bound can be found. By taking equation (4.2)

$$\|Su\|_{L^p(\Gamma)} = \left(\int_{\Gamma} \left| \int_{\Gamma} \kappa(x, y) u(y) ds(y) \right|^p ds(x) \right)^{\frac{1}{p}}$$

and the Hölder Inequality for Integrals (taken from [4])

$$\left| \int_a^b f(x)g(x)dx \right| \leq \left[\int_0^b |f(x)|^c dx \right]^{\frac{1}{c}} \left[\int_a^b |g(x)|^d dx \right]^{\frac{1}{d}}$$

if

$$\frac{1}{c} + \frac{1}{d} = 1, c > 1, d > 1.$$

we get

$$\|Su\|_{L^p(\Gamma)} \leq \left(\int_{\Gamma} \left[\left(\int_{\Gamma} |\kappa(x, y)|^q ds(y) \right)^{\frac{1}{q}} \left(\int_{\Gamma} |u(y)|^p ds(y) \right)^{\frac{1}{p}} \right]^p ds(x) \right)^{\frac{1}{p}}$$

with

$$\|u\|_{L^p} = \left(\int_{\Gamma} |u(y)|^p \right)^{\frac{1}{p}}.$$

Then

$$\begin{aligned} \|Su\|_{L^p(\Gamma)} &= \left(\int_{\Gamma} \left(\left(\int_{\Gamma} |\kappa(x, y)|^q ds(y) \right)^{\frac{1}{q}} \|u\|_{L^p} \right)^p ds(x) \right)^{\frac{1}{p}} \\ &\leq \left(\int_{\Gamma} \left(\int_{\Gamma} |\kappa(x, y)|^q ds(y) \right)^{\frac{p}{q}} ds(x) \right)^{\frac{1}{p}} \|u\|_{L^p} \end{aligned}$$

where the $\|u\|_{L^p}$ has been taken out of the integration since it is independent of x . This can then be written

$$\|S\|_{L^p} \leq \left(\int_{\Gamma} \left(\int_{\Gamma} |k(x, y)|^q ds(y) \right)^{\frac{p}{q}} ds(x) \right)^{\frac{1}{p}}$$

for $1 < p < \infty$ and requiring

$$\frac{1}{p} + \frac{1}{q} = 1, \text{ i.e. } q = \frac{p}{p-1}.$$

Giving the following upper bound after parameterising x and y over the interval $[0, 2\pi]$,

$$\|S\|_{L^p} \leq \left(\int_0^{2\pi} \left(\int_0^{2\pi} |\kappa(t, \tau)|^q |y'(\tau)| d\tau \right)^{\frac{p}{q}} |y'(t)| dt \right)^{\frac{1}{p}}. \quad (4.13)$$

This upper bound gives us Figure 4.3 for $k = 1$.

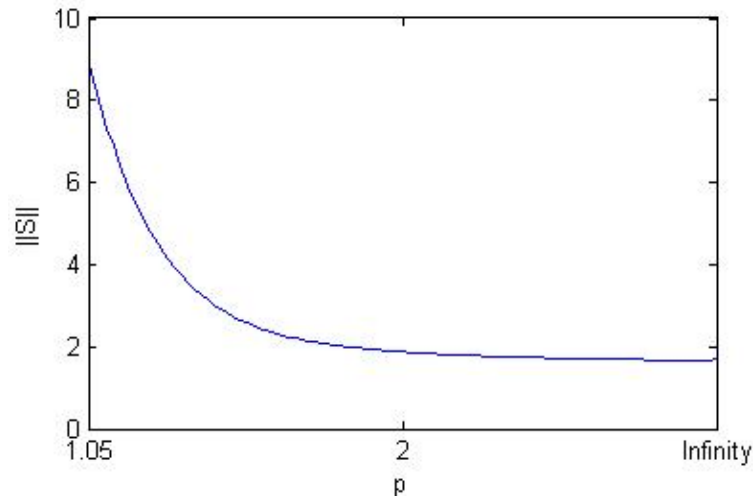


Figure 4.3: Upper bound 4.13 for $1 \leq p \leq \infty$ and $k = 1$

Another upper bound can be obtained from the Riesz-Thorin interpolation (see Theorem 5.13 in [5]),

$$\|S\|_{L^p} \leq \|S\|_{L^1}^{\frac{1}{p}} \cdot \|S\|_{L^\infty}^{1-\frac{1}{p}}. \quad (4.14)$$

Figure 4.4 shows the upper bound this generates. However, since the 1-norm and the ∞ -norm are the same, this just gives a straight line. By taking the upper bounds (4.13) and (4.14) together and using the smaller values we get Figure 4.5. Furthermore, using the result from equation (4.8) we can make the figure symmetric about $p = 2$, giving us Figure 4.6. The Riesz-Thorin interpolation can then be used again, so we finally get the upper bound in 4.7.

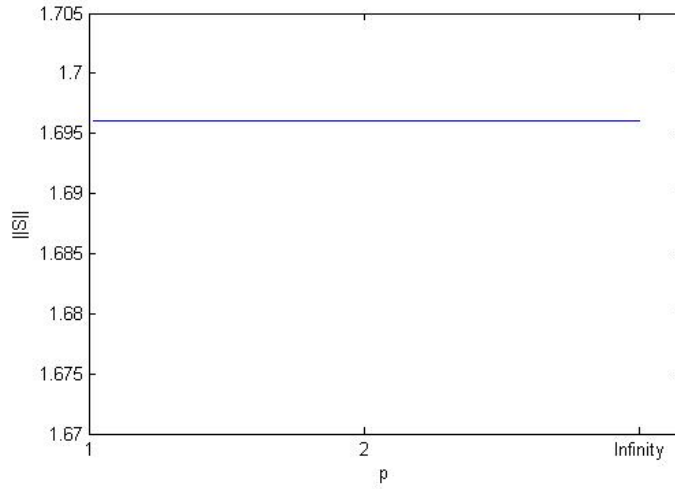


Figure 4.4: Upper bound Using the Riesz-Thorin Interpolation 4.14 for $k = 1$

5 Lower Bounds on $\|S\|_{L^p}$

The lower bound for the 2-norm can be found by looking at equation (4.4).

Letting $p = 2$ we have the following,

$$\|S\|_{L^2[0,2\pi]} = \sup_{\|u\|_{L^2}=1} \left(\int_0^{2\pi} \left| \int_0^{2\pi} \kappa(t, \tau) u(\tau) |y'(\tau)| d\tau \right|^2 |y'(t)| dt \right)^{\frac{1}{2}}. \quad (5.1)$$

Alternatively, we can have

$$\|S\|_{L^2[0,2\pi]} = \sup_{u \neq 0} \frac{\|Su\|_{L^2}}{\|u\|_{L^2}}. \quad (5.2)$$

Unlike for the 1-norm and the ∞ -norm this cannot be simplified into a single integral, and also there is no obvious u to take in finding the supremum of $\frac{\|Su\|_{L^2}}{\|u\|_{L^2}}$. Hence, in looking at finding values for the lower bound we should

try as many different u as possible. Choosing piecewise constant u , we can split the inner integral up and use a similar method to that of the 1-norm.

We can have

$$\|Su\|_{L^2} = \left(\int_0^{2\pi} \left| \sum_{j=1}^N \int_{a_j}^{b_j} \kappa(t, \tau) U_j |y'(\tau)| d\tau \right|^2 |y'(t)| dt \right)^{\frac{1}{2}}$$

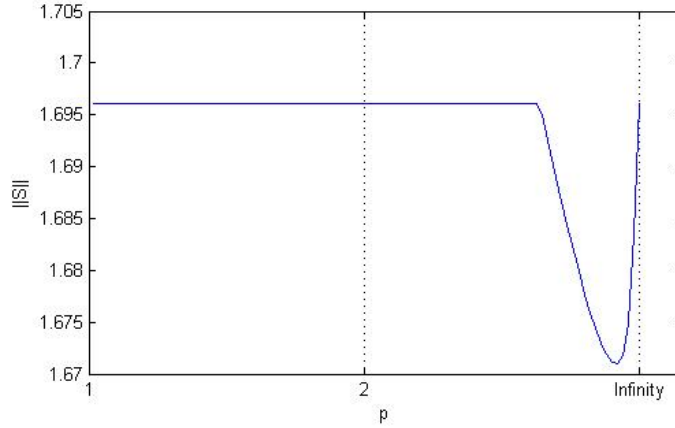


Figure 4.5: Combined Upper Bounds from Figures 4.4 and 4.3 for $k = 1$

where $a_j = \frac{(j-1)2\pi}{N}$, $b_j = \frac{j2\pi}{N}$ and U_j is a constant. The constants are chosen randomly over a uniform distribution, and are of the form,

$$U_j = A_j + B_j i, \text{ with } A, B \in [-1, 1], i = \sqrt{-1}.$$

Then we also have,

$$\|u\|_{L^2} = \left(\sum_{j=1}^N \int_{a_j}^{b_j} |U_j|^2 |y'(\tau)| \right)^{\frac{1}{2}}$$

which gives us an lower bound for $\|S\|_{L^2[0,2\pi]}$. Using this technique Table 5.1 shows the lower bound values that were found.

6 Numerical Methods for the Lower and Upper Bounds

All integrals we approximated using *Legendre Gaussian Quadrature*. Although, for highly oscillatory functions such as the Hankel function this does not give exactness, all results shown have converged as in 6.3. We begin this section by giving an overview of Gaussian Quadrature.

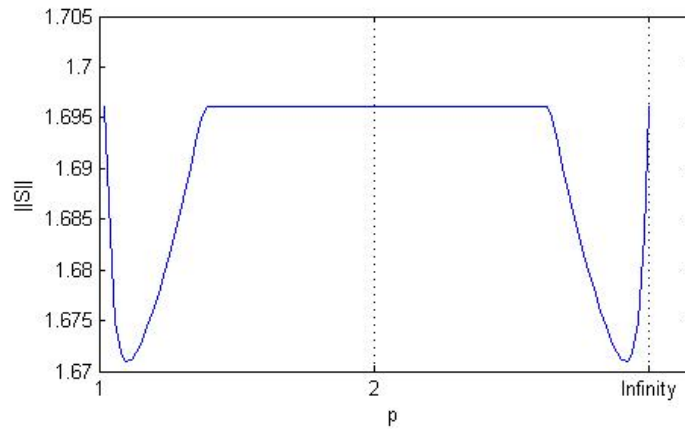


Figure 4.6: Upper Bound using the Symmetric Property for Figure 4.5

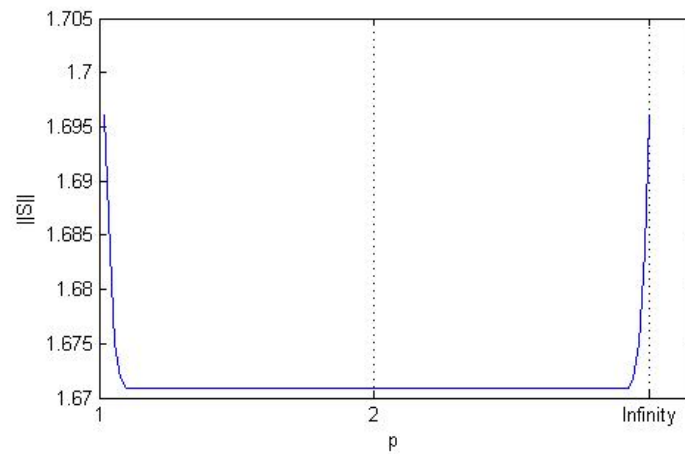


Figure 4.7: Symmetric Upper Bound for $k = 1$ Using 4.14 Again

k	$\ S\ _{L^2}$ Lower Bound for $y(\tau) = (\cos \tau, \sin \tau)$	$\ S\ _{L^2}$ Lower Bound for $y(\tau) = (2 \cos \tau, \sin \tau)$
1	0.92591123989195	0.91814408816802
2	0.48317060607222	0.54140030886589
4	0.24311615739346	0.26110271592417
8	0.11254776960321	0.13052717540095
16	0.05744056422210	0.07149107040318
32	0.02268706077302	0.03127729495608

Table 5.1: Lower Bound Numeric Approximations for the 2-norm

6.1 Gaussian Quadrature

Gaussian Quadrature is a type of numerical integration. The likes of the *Simpson Rule* and the *Trapezoidal Rule* converge much slower for almost all functions. With the Simpson Rule being accurate for quadratic curves between nodes, and the Trapezoidal Rule being accurate for linear curves between nodes. Gaussian Quadrature is based around taking the roots of a specific polynomial and using this to decide which points to use. This is the difference between the Simpson and Trapezoidal rules which always take the points at the beginning and end of the interval. There are many types of Gaussian Quadrature methods, dependent on the polynomial used. Hermite Gaussian Quadrature is based around the Hermite polynomials. The method used in this project was *Legendre Gaussian Quadrature*, and is therefore based around the Legendre polynomials (6.1). With the points used for the Gaussian Quadrature being the roots of the Legendre polynomial (6.2). The aim of the Gaussian Quadrature method is to give an exact result for

polynomials of degree $2n - 1$ with n being the number of points used.

6.1.1 Legendre Polynomial

The Legendre polynomials provide one option for the weights and points to be used for Gaussian Quadrature. The Legendre polynomials are an infinite set of orthogonal polynomials on the interval $(-1, 1)$ with respect to the weight function $w(x) \equiv 1$. These polynomials are the solution of Legendre's differential equation,

$$\frac{d}{dx} \left[(1 - x^2) \frac{d}{dx} P(x) \right] + n(n + 1)P(x) = 0 \quad (6.1)$$

They can be expressed using *Rodrigues' formula* [4]

$$P_n(x) = (2^n n!)^{-1} \frac{d^n}{dx^n} [(x^2 - 1)^n]. \quad (6.2)$$

Hence the first four are:

$$\begin{aligned} P_0(x) &= 1 \\ P_1(x) &= x \\ P_2(x) &= \frac{3}{2}x^2 - \frac{1}{2} \\ P_3(x) &= \frac{5}{2}x^3 - \frac{3}{2}x \end{aligned}$$

6.2 How Gaussian Quadrature Works in 1-D

Gaussian Quadrature approximates a function $f(x)$ on a defined interval $[a, b]$ say. This function is ideally continuous. However, if it is not but it is known where the function is not continuous the interval can be split up to avoid the discontinuity¹. We require

¹Of course notice should be made that the discontinuous area is an important part of the integration, and would be foolish to ignore off hand.

$$\int_b^a f(x)dx \approx \sum_{i=1}^n w_i f(x_i) \quad (6.3)$$

The weights w_i and points x_i are determined by the polynomial used. The domain usually taken for the rule is $[-1, 1]$, and therefore requires a transformation for a general $[a, b]$ domain where $a, b \in \mathbb{R}$. This is done by

$$\int_a^b f(x)dx = \frac{b-a}{2} \int_{-1}^1 f\left(\frac{b-a}{2}x + \frac{a+b}{2}\right) dx$$

which after applying the Gaussian quadrature rule is

$$\frac{b-a}{2} \sum_{i=1}^n w_i f\left(\frac{b-a}{2}x_i + \frac{a+b}{2}\right). \quad (6.4)$$

The accuracy of Gaussian Quadrature (provides the exact value of a polynomial of degree $(2n - 1)$ with n Gaussian Quadrature points and weights) is managed by the way that the n weights and n points can be chosen. Since there are $2n$ parameters to choose and a polynomial of $(2n - 1)$ also has $2n$ parameters, it can be seen why a n th Gaussian quadrature can not give greater accuracy. Looking at a specific example can show how the points and weights are chosen as to give optimum exactness.

6.2.1 Example

Taking $n = 3$ and the interval $[-1, 1]$ then the weights w_1, w_2 and w_3 and the points x_1, x_2 and x_3 need to be chosen such that,

$$\int_{-1}^1 f(x)dx = w_1 f(x_1) + w_2 f(x_2) + w_3 f(x_3).$$

Since $n = 3$ it is required to give exactness for a polynomial of degree 5 (i.e. $2n - 1 = 2(3) - 1 = 5$), then

$$f(x) = a_0 + a_1x + a_2x^2 + a_3x^3 + a_4x^4 + a_5x^5$$

where a_0, a_1, \dots, a_5 are constants (noticing there are the same number of constants as there are weights and points). Therefore it is needed that,

$$\int (a_0 + a_1x + \dots + a_5x^5)dx = a_0 \int 1dx + a_1 \int xdx + \dots + a_5 \int x^5dx$$

which is equivalent to showing that the Gaussian quadrature method gives exact results when $f(x) = 1, x, \dots, x^5$. Thus we need,

$$\begin{aligned} w_1 + w_2 + w_3 &= \int_{-1}^1 1dx = 2 \\ w_1x + w_2x + w_3x &= \int_{-1}^1 xdx = 0 \\ w_1x^2 + w_2x^2 + w_3x^2 &= \int_{-1}^1 x^2dx = \frac{2}{3} \\ w_1x^3 + w_2x^3 + w_3x^3 &= \int_{-1}^1 x^3dx = 0 \\ w_1x^4 + w_2x^4 + w_3x^4 &= \int_{-1}^1 x^4dx = \frac{2}{5} \\ w_1x^5 + w_2x^5 + w_3x^5 &= \int_{-1}^1 x^5dx = 0. \end{aligned}$$

This system of equations has the unique solution,

$$x_1 = -0.77459666924148, x_2 = 0, x_3 = 0.77459666924148$$

$$w_1 = 0.555555555555556, w_2 = 0.888888888888889, w_3 = 0.555555555555556,$$

where the x_i are the roots of $P_3(x) = 0$. This works for all n , and a proof for all n can be found in [6].

6.2.2 2-D Gaussian Quadrature

A simple extension of the method used for single integrals is required to integrate a double integral using Gaussian Quadrature. For the double integral we have

$$\int_{-1}^1 f(x, y) dx dy = \sum_{j=1}^m \sum_{i=1}^n w_i v_j f(x_i, y_j) dx dy$$

where the w_i and the x_i are the weights and the points in the x direction and the v_j and the y_j are the weights and the points in the y direction . This double integral again needs to be transformed into the interval $[a, b] \times [c, d]$. This is done in a similar way to before.

$$\int_a^b f(x, y) dx dy = \sum_{j=1}^m \sum_{i=1}^n w_i v_j f\left(\frac{b-a}{2}x_i + \frac{b+a}{2}, \frac{d-c}{2}y_j + \frac{d+c}{2}\right) dx dy \quad (6.5)$$

6.3 Testing the Method

According to the theory if I take n Gaussian quadrature points over the interval $[-1, 1]$ then this should give the exact value for a polynomial of order $2n - 1$. Thus if I take $n = 2$ then this should give the exact value for any cubic. By taking many different n and testing the MATLAB code we have written on the relevant polynomial we can test if the code is correct and that the Gaussian Quadrature method is working. Looking at the values in Table 6.1 where n Gaussian Quadrature points and $(n - 1)$ Gaussian Quadrature points have been used, and the interval $[-2, 3]$ you can see that a polynomial of order $2n - 1$ is integrated correctly for n points but not for $(n - 1)$ points. Also notice how the accuracy improves for a function such as sin and cos as n increases. Testing the double integral code is also necessary. Choosing $a = 1, b = 2, c = 3$ and $d = 4$ and increasing n and m as we increase the order of the polynomials lets us see whether the code is as accurate as it should be. (See Table 6.2)

Polynomial	Exact Value	n	n Points	$(n - 1)$ Points
$2x^3 + x^2 - 2$ (cubic)	34.1667	2	34.1667	-7.5000
$-x^5 + 3x^4$ (quintic)	54.1667	3	54.1667	45.4861
$7x^7 + 7x^6$ (7 th order)	7831.87	4	7831.87	6952.96
$\sin(x) + \cos(x)$	1.62426	5	1.62428	1.62298

Table 6.1: Single Integral Gaussian Quadrature Code

Polynomial	Exact Value	n, m	n, m Points	$(n - 1), (m - 1)$ Points
$x^3 + y^3$	47.5	2, 2	47.500	46.250
$x^5 + y^5$	571.667	3, 3	571.667	571.569
$x^7 - y^7$	-7.34000	4, 4	-7.34000	-7.33999
$\sin(x) + \cos(y)$	-0.268522	3, 3	-0.268522	-0.268442

Table 6.2: Double Integral Gaussian Quadrature Code

6.4 Evaluating the Single Integral

We have the two single integrals

$$\|S\|_{L^1(\Gamma)} = \sup_{\tau \in [0, 2\pi]} \int_0^{2\pi} \left| \frac{i}{4} H_0^1(k|y(t) - y(\tau)|) |y'(t)| \right| dt \quad (6.6)$$

$$\|S\|_{L^\infty(\Gamma)} = \sup_{t \in [0, 2\pi]} \int_0^{2\pi} \left| \frac{i}{4} H_0^1(k|y(t) - y(\tau)|) |y'(\tau)| \right| d\tau. \quad (6.7)$$

We have H_0^1 as the Hankel function, this is made up of the first kind and second kind Bessel functions. $y(\tau)$ represents the shape which we are looking at, for instance in the circle case we have $y(\tau) = (\cos(\tau), \sin(\tau))$. In this case the $|y'(\tau)|$ term would be $\sqrt{\cos^2(\tau) + \sin^2(\tau)}$. Also, there is the $|y(t) - y(\tau)|$

term. This term is the vector modulus of $y(t) - y(\tau)$. Thus for the circle

$$|y(t) - y(\tau)| = \left| \begin{array}{c} \cos(t) - \cos(\tau) \\ \sin(t) - \sin(\tau) \end{array} \right| = \sqrt{(\cos(t) - \cos(\tau))^2 + (\sin(t) - \sin(\tau))^2}.$$

Performing some manipulation,

$$\sqrt{(\cos(t) - \cos(\tau))^2 + (\sin(t) - \sin(\tau))^2} = \sqrt{2 - 2\cos(t - \tau)}$$

Then using the trigonometric identity $\sin^2(x) = \frac{1 - \cos(2x)}{2}$,

$$\begin{aligned} \sqrt{(\cos(t) - \cos(\tau))^2 + (\sin(t) - \sin(\tau))^2} &= \sqrt{4\sin^2\left(\frac{t - \tau}{2}\right)} \\ &= 2\sin\left|\frac{t - \tau}{2}\right| \end{aligned}$$

The method chosen to numerically integrate these integrals was Legendre Gaussian Quadrature. This can then be programmed in MATLAB. The idea of the program was for the y (= shape of object) to be input, i.e. so that the shape can be easily changed. Running the program we should have convergence as the number of points (n) used for the Gaussian Quadrature increases. Taking different values of k = wave number, t = start point on the shape and n , we obtained Table 6.3.

As wanted and expected with k increasing we get ever decreasing values. With a circle being symmetric the values of t should not affect the values that we converge to. Looking at Table 6.4 we can see the only difference is the rate of convergence. This can be explained by the method that is being used. Since Gaussian Quadrature will have different points depending on where t is, and hence will have different values dependent on how near the points are to the singularity.

n	$k = 1$	$k = 2$	$k = 64$
8	1.25599845796364	0.92636623468931	0.17206436985466
16	1.26820470397750	0.93836905487429	0.17805048230319
32	1.27153224321317	0.94166907961211	0.18061491732263
64	1.27240328043588	0.94253590847969	0.18141859166216
128	1.27262646245432	0.94275842180936	0.18163342024274
256	1.27268300857123	0.94281485758333	0.18168871333813
512	1.27269725094977	0.94282908104077	0.18170275604897
1024	1.27270082697329	0.94283265370303	0.18170629876787
2048	1.27270172332930	0.94283354944311	0.18170718933635
4096	1.27270194779501	0.94283377379287	0.18170741275990
8192	1.27270200397511	0.94283382995065	0.18170746874657
16384	1.27270201803147	0.94283384400261	0.18170748276610
32768	1.27270202154766	0.94283384751793	0.18170748627512

Table 6.3: Approximations of $\|S\|_{L^1} = \|S\|_{L^\infty}$ for a Circle with $t = 0$

7 Speeding Up the Code

There are two key ways that the code has been improved. This is by using vectors and matrices instead of *for* loops, and also by using a graded mesh.

7.1 *For* Loops vs Vectors and Matrices

In MATLAB *for* loops are computed significantly slower than multiplying vectors and matrices. This is because MATLAB was originally designed to

n	$t = \frac{\pi i}{4}$	$t = \frac{\pi}{2}$	$t = \frac{3\pi}{2}$	$t = 2\pi = 0$
1024	1.2722513420	1.2716660046	1.2722513420	1.2727008269
2048	1.2731297511	1.2721816171	1.2731297511	1.2727017233
4096	1.2725886266	1.2724409165	1.2725886266	1.2727019477
8192	1.2728096451	1.2725711201	1.2728096451	1.2727020039
16384	1.2726735661	1.2726364333	1.2726735661	1.2727020180
32768	1.2727290360	1.2726691723	1.2727290360	1.2727020215

Table 6.4: Approximations of $\|S\|_{L^1} = \|S\|_{L^\infty}$ for Different t for a Circle

manipulate vectors and matrices, e.g. finding inverses, and therefore needed to do this efficiently. A *for* loop can be written equivalently by using a vector multiplied by another vector. This can be seen clearly by taking an example of the code that was used in computing Gaussian Quadrature integration for the single integral, i.e. to evaluate $\int_a^b f(t, \tau, k) d\tau \approx \sum_{j=1}^n w_j f(t_j, \tau_j, k)$.

```
for 1:n;
    h = h + w(i)*f(t(i),tau,k)
end
```

This can be re-written using two vectors,

```
w*f(t,tau,k)
```

What is going on above can be expressed as,

$$\begin{pmatrix} w(1) & w(2) & \dots & w(n) \end{pmatrix} \begin{pmatrix} f(t(1), \tau, k) \\ f(t(2), \tau, k) \\ \dots \\ f(t(n), \tau, k) \end{pmatrix}.$$

Similarly, two *for* loops can be written by *vector* \times *matrix* \times *vector*. Taking another example of code that was used,

```
for i = 1:m;
    for j = 1:n;
        h = h + w(i)*f(t(i),tau(j),k);
    end
    g = g + v(j)*h;
end
```

can be re-written,

```
w*f(t,tau,k)*v;
```

where $f(t, \tau, k)$ is the matrix

$$f(t, \tau, k) = \begin{pmatrix} f(t(1), \tau(1), k) & \dots & f(t(1), \tau(m), k) \\ f(t(2), \tau(1), k) & \dots & f(t(2), \tau(m), k) \\ f(t(3), \tau(1), k) & \dots & f(t(3), \tau(m), k) \\ \vdots & & \vdots \\ f(t(n), \tau(1), k) & \dots & f(t(3), \tau(m), k) \end{pmatrix}$$

The matrix is found by some manipulation of the vectors that contain the weights and points required in Gaussian Quadrature.

7.2 Graded Mesh - The Duffy Transformation

With a singularity slicing the region that is being integrated in two as shown in (7.1), using a graded mesh as we approach the singularity is difficult. However, by transferring this region into two rectangles which has singularities

on the edges a graded mesh can be used. The original double integral (4.4)

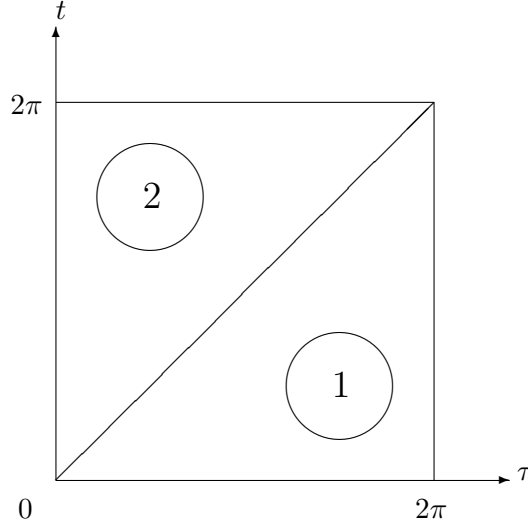


Figure 7.1: Region Before Transformation

can be written,

$$\begin{aligned} & \left(\int_0^{2\pi} \left| \int_0^{2\pi} F(t, \tau) |y'(\tau)| d\tau \right|^p |y'(t)| dt \right) \\ &= \left(\int_0^{2\pi} \left| \int_0^\tau F(t, \tau) |y'(t)| dt \right|^p |y'(\tau)| d\tau \right. \\ & \quad \left. + \int_0^{2\pi} \left| \int_0^t F(t, \tau) |y'(\tau)| d\tau \right|^p |y'(t)| dt \right) \end{aligned}$$

where $F(t, \tau) = \frac{i}{4} H_0^1(k|y(t) - y(\tau)|)$. For the Gaussian Quadrature method, we need to make sure that the correct points are taken from the intervals. Triangle 1 takes points using the integral $\int_0^{2\pi} \left| \int_0^\tau F(t, \tau) |y'(t)| dt \right|^p |y'(\tau)| d\tau$ and triangle 2 takes points using $\int_0^{2\pi} \left| \int_0^t F(t, \tau) |y'(\tau)| d\tau \right|^p |y'(t)| dt$.

Taking the *Duffy Transformation* $\tau = st$, $\frac{d\tau}{ds} = t$ triangle 2 becomes a rectangle as in Figure 7.2. The singularities being where $\tau = t$ are therefore now at $s = 1$ and $t = 0$. After this transformation there is the integral

$$\int_0^{2\pi} \left| \int_0^1 F(t, st) |y'(st)| t ds \right|^p |y'(t)| dt \quad (7.1)$$

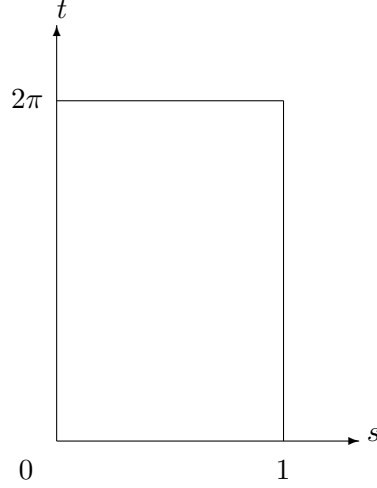


Figure 7.2: Transformed Triangle 2

for triangle 2. The use of a graded mesh is now a lot simpler. Using four different meshes on the rectangle it is possible to have many points near the singularity points, and save on expense by using relatively few points far away from the singularity. Dividing the rectangle as follows (shown in Figure 7.3):

- In the region, $[0, \frac{k-1}{k}] \times [\frac{2\pi}{k}, 2\pi]$ using n by n Gaussian Quadrature points in each dotted area shown in Figure 7.3..
- In the region, $[0, \frac{k-1}{k}] \times [0, \frac{2\pi}{k}]$ using n Gaussian Quadrature points in the s direction. With n Gaussian points every $[\frac{2\pi}{k}(0.15^i), \frac{2\pi}{k}(0.15^{i+1})]$ with $i = \{0, 1, \dots, 9\}$ in the t direction for each dotted area.
- In the region, $[\frac{k-1}{k}, 1] \times [\frac{2\pi}{k}, 2\pi]$ using n Gaussian Quadrature points in the t direction. With n Gaussian Quadrature points every $[1 - \frac{0.15^i}{k}, 1 - \frac{0.15^{i+1}}{k}]$ with $i = \{0, 1, \dots, 9\}$ in the s direction for each dotted area.

- In the region, $[\frac{k-1}{k}, 1] \times [0, \frac{2\pi}{k}]$ there is a fine mesh in both directions. With n Gaussian Quadrature points every $[1 - \frac{0.15^i}{k}, 1 - \frac{0.15^{i+1}}{k}]$ with $i = \{0, 1, \dots, 9\}$ in the s direction and n Gaussian Quadrature points every $[\frac{2\pi}{k}(0.15^i), \frac{2\pi}{k}(0.15^{i+1})]$ with $i = \{0, 1, \dots, 9\}$ in the t direction.

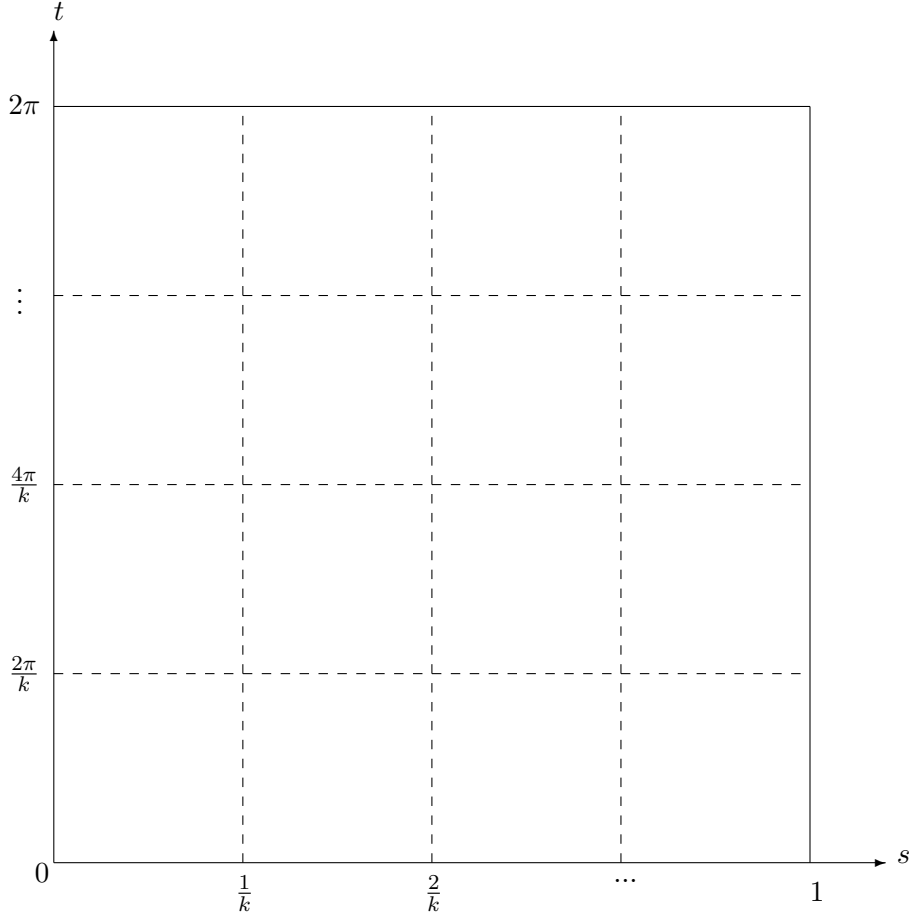


Figure 7.3: The Divided Mesh Used for Triangle 2

There are two reasons why the Duffy Transformation is useful here. Firstly, we have divided the mesh so that there is always n points per wavelength. This deals with the oscillations. These oscillations (especially with large k) mean that the Gaussian Quadrature method is less accurate. Hence, without the number points (n) increasing with k the accuracy would decline. Secondly, we are also concentrating the points near the singularity using the

graded mesh. This means that where a lot is going on, we are concentrating a lot of our resources. Therefore the larger oscillations near the singularity can be approximated with greater accuracy.

7.3 The Duffy Transformation for Piecewise Constants

If the τ axis is split up into evenly spaced piecewise constants (see Figure 4.2) then the Duffy transformation can still be used. The transformation works when both integrals start at zero. Taking the j th piecewise constant from a_j to b_j , then we have the rectangular area as shown in Figure 7.3 from a_j to b_j on the τ axis and 0 to 2π on the t axis. This can be split into three separate double integrals,

$$\int_0^{2\pi} \int_{a_j}^{b_j} = \int_0^{a_j} \int_{a_j}^{b_j} + \int_{a_j}^{b_j} \int_{a_j}^{b_j} + \int_{b_j}^{2\pi} \int_{a_j}^{b_j}.$$

With $\int_0^{a_j} \int_{a_j}^{b_j}$ and $\int_{b_j}^{2\pi} \int_{a_j}^{b_j}$ able to be done normally just by using n Gaussian quadrature in the t and τ directions. The other integral from $\int_{a_j}^{b_j} \int_{a_j}^{b_j}$ is to be done using the Duffy transformation. Thus we have the two triangles again, taking triangle 2 we have the integral,

$$\int_{a_j}^{b_j} \left| \int_{a_j}^t \kappa(t, \tau) |y'(\tau)| d\tau \right| |y'(t)| dt.$$

Since, the integral starts at $a_j \neq 0$ (except for the first j), another transformation needs to be done, before the Duffy transformation. Hence, by letting $\tilde{t} = t - a_j$ and $\tilde{\tau} = \tau - a_j$ then,

$$\begin{aligned} & \int_{a_j}^{b_j} \left| \int_{a_j}^t \kappa(t, \tau) |y'(\tau)| d\tau \right| |y'(t)| dt \\ &= \int_0^{b_j - a_j} \left| \int_0^{\tilde{t}} \kappa(\tilde{t} + a_j, \tilde{\tau} + a_j) |y'(\tilde{\tau} + a_j)| d\tilde{\tau} \right| |y'(\tilde{t} + a_j)| d\tilde{t} \\ &= \int_0^{b_j - a_j} \left| \int_0^t \kappa(t + a_j, \tau + a_j) |y'(\tau + a_j)| d\tau \right| |y'(t + a_j)| dt. \end{aligned}$$

Now, performing the Duffy transformation as before by letting $\tau = st$, $\frac{d\tau}{ds} = t$ this becomes,

$$\int_0^{b_j - a_j} \left| \int_0^1 \kappa(t + a_j, st + a_j) |y'(st + a_j)| t ds \right| |y'(t + a_j)| ds.$$

This is a rectangle similar to before, where the singularities are at $t = 0$ and $s = 1$, and the grading can be done as before.

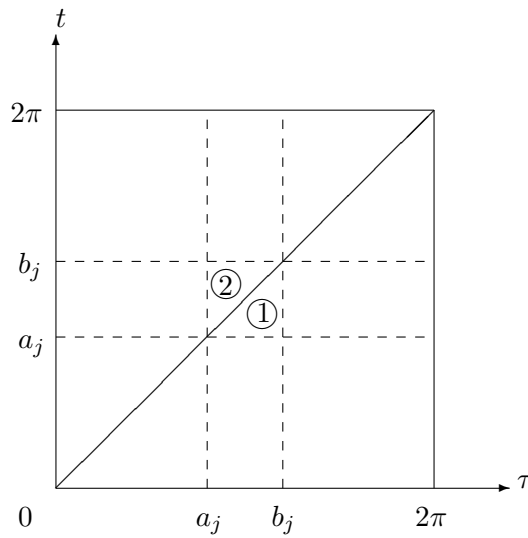


Figure 7.4: Region Before Transformation Using Piecewise Constants

8 Results

We have 1-norm and ∞ -norm results for the operator S (i.e. $\|S\|_{L^1}$ and $\|S\|_{L^\infty}$). Using these results (shown in Table 8.1) we are able to say how the $\|S\|$ changes as we increase k for the circle. Table 8.2 shows this for an ellipse of the form $y(\tau) = (2 \cos \tau, \sin \tau)$. Upper bounds (Figure 8.1) and lower bounds (Table 5.1) found in Sections 4 and 5 can be used together, and by analysing the region in which the 2-norm can lie, results can be gathered (Table 8.3 and Table 8.4) to determine behaviour of $\|S\|_{L^2}$.

8.1 1-norm and the ∞ -norm

Using the single integrals it was possible to look at how the values changed as k was increased. Looking at the circle first we obtain Table 8.1. From this it can be seen that $\log_k \|S\|_k$ approaches -0.5 as k becomes very large (i.e. approaches infinity). We require the result $\|S\| \propto k^\alpha$ for some α to be found. The following argument, resulting in equation (8.1), allows us to conclude that this value of α is $-\frac{1}{2}$. We have,

$$\|S\| \propto k^\alpha \Rightarrow C \leq \frac{\|S\|_k}{k^\alpha} \leq D$$

then multiplying through by k^α ,

$$Ck^\alpha \leq \|S\|_k \leq Dk^\alpha \text{ where } C \text{ and } D \text{ are constants.}$$

Next we take \log_k ,

$$\log_k Ck^\alpha \leq \log_k \|S\|_k \leq \log_k Dk^\alpha$$

which can be rearrange to the following by use a log properties,

$$\log_k C + \alpha \leq \log_k \|S\|_k \leq \log_k D + \alpha.$$

By taking the limit as $k \rightarrow \infty$ we have,

$$0 + \alpha \leq \log_k \|S\|_k \leq 0 + \alpha \text{ as } k \rightarrow \infty.$$

and lastly we can squeeze this to get the result,

$$\log_k \|S\|_k = \alpha \text{ as } k \rightarrow \infty. \tag{8.1}$$

k	$\ S\ _{L^1}$ for $y(\tau) = (\cos \tau, \sin \tau)$	$\log_k \ S\ _{L^1}$ for $y(\tau) = (\cos \tau, \sin \tau)$
1	1.27269909813074	-
2	0.94283092667553	-0.08492901233913
4	0.68817972895875	-0.26957134912594
8	0.49731659257114	-0.33592117619175
\vdots	\vdots	\vdots
512	0.06497404812582	-0.43822139961133
1024	0.04602585988168	-0.44414115146863
2048	0.03258593605505	-0.44905515924963
\vdots	\vdots	\vdots
32768	0.00816349758682	-0.46243979257239
65536	0.00577323389157	-0.46477528813075
131072	0.00408254822470	-0.46684202100476

Table 8.1: Approximation to the 1-norm for the Circle as $k \rightarrow \infty$ using the Single Integral

k	$\ S\ _{L^1}$ for $y(\tau) = (2 \cos \tau, \sin \tau)$	$\log_k \ S\ _{L^1}$ for $y(\tau) = (2 \cos \tau, \sin \tau)$
1	1.69610277091235	-
2	1.24342380180744	0.314318100540
4	0.90092608453265	-0.075259674143
8	0.64775084718857	-0.208829699197
\vdots	\vdots	\vdots
512	0.08377570223088	-0.397480479470
1024	0.05931984422385	-0.407534138055
2048	0.04198543625736	-0.415815201043
\vdots	\vdots	\vdots
32768	0.01051196564617	-0.438121581588
65536	0.00743359297322	-0.44198278682149
131072	0.00408254822470	-0.44539334859934

Table 8.2: Results for the 1-Norm as $k \rightarrow \infty$ for $y(\tau) = (2 \cos \tau, \sin \tau)$ using the Single Integral

k	$\ S\ _{L^2}$ for $y(\tau) = (2 \cos \tau, \sin \tau)$	$\log_k \ S\ _{L^2}$ for $y(\tau) = (2 \cos \tau, \sin \tau)$
1	1.294548530868040	-
2	0.883817805885845	-0.178179098161715
4	0.575077907006125	-0.399085340338845
8	0.384944183600455	-0.459092940931912
16	0.264450390167755	-0.479732747741775
32	0.178648232053725	-0.496961291630781

Table 8.3: Approximations for the 2-Norm as $k \rightarrow \infty$ for $y(\tau) = (2 \cos \tau, \sin \tau)$ using the mid-point of the lower and upper bounds

k	$\ S\ _{L^2}$ for $y(\tau) = (2 \cos \tau, \sin \tau)$	$\log_k \ S\ _{L^2}$ for $y(\tau) = (2 \cos \tau, \sin \tau)$
1	1.099302310682300	-
2	0.712985616473335	-0.488055122358312
4	0.465608077134420	-0.551406004638562
8	0.304862263350300	-0.571256838020022
16	0.207136917659770	-0.567835847333577
32	0.138804079212980	-0.569775625604814

Table 8.4: Approximations for the 2-Norm as $k \rightarrow \infty$ for the circle using the mid-point of the lower and upper bounds

8.2 The 2-norm

The upper bounds and lower bounds found in Sections 4 and 5 allow us to investigate the 2-norm. The upper bounds for the circle as k increase can be seen in Figure 8.2, and for the ellipse $y(\tau) = (2 \cos \tau, \sin \tau)$ can be seen in Figure 8.1. The lower bounds as k increase can be seen in Table 5.1. Using these bounds we then have a region where the 2-norm must lie. By taking the mid-point of this region, we can use them to calculate a table as we did for the 1-norm and the ∞ -norm. This Table 8.3 shows results for the ellipse. Taking the mid-point as we increase k the value of $\log_k \|S\|_{L^2}$ seems to be approaching $-\frac{1}{2}$. Table 8.4 shows results for the circle, where again the

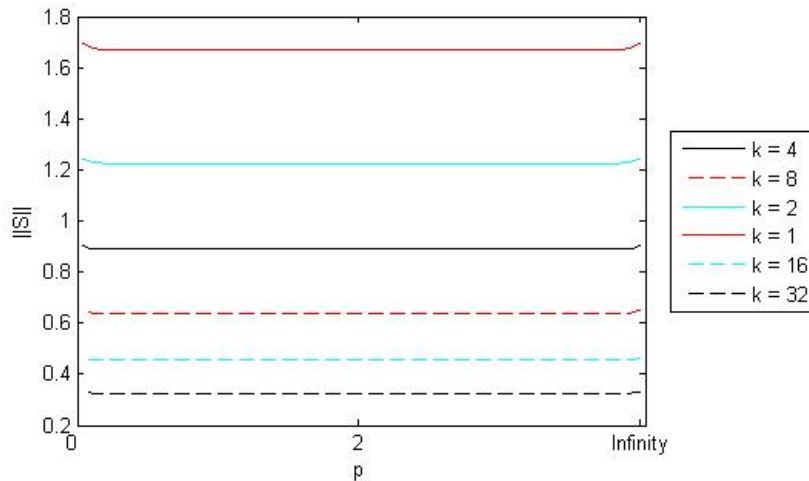


Figure 8.1: Upper Bounds of $\|S\|_{L^p}$ with k increasing for $y(\tau) = (2 \cos \tau, \sin \tau)$

mid-point of the upper and lower bound for $\|S\|_{L^2}$ has been taking. This time the value seems to be larger than $-\frac{1}{2}$.

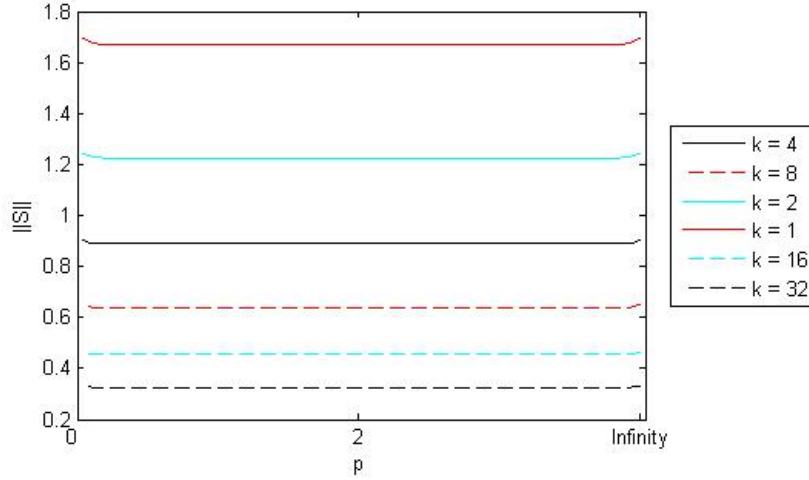


Figure 8.2: Upper Bounds of $\|S\|_{L^p}$ with k increasing for the Circle

9 Conclusion

The aim of this project was to look at behaviour of the single layer potential, S , which would be a crucial step in analysing the operator A and its asymptotics as the wavenumber k goes to infinity. The numerical results indicate that $\|S\|_{L^1}$ and $\|S\|_{L^\infty}$ behave like $k^{-\frac{1}{2}}$ for a circle and an ellipse. However, we want to make conclusions about the operator A . We have that

$$A = I + 2D + 2i\eta S.$$

Therefore, by choosing $\eta = k$ as in [1] then

$$2i\eta S = 2ikS$$

which behaves like $k^{\frac{1}{2}}$.

By using our upper and lower bounds, we are able to indicate where the 2-norm lies. In taking the mid-point and looking at the \log_k of this as k increases we can see that for our ellipse these values behave like $k^{-\frac{1}{2}}$. Assuming the mid-point is a good approximation to $\|S\|_{L^2}$ we can estimate

that $\|S\|_{L^2}$ behaves like $k^{-\frac{1}{2}}$. Then by choosing $\eta = k$ again, this tells us that we have behaviour of $\|A\|_{L^2}$ like $k^{\frac{1}{2}}$. This is the same result as stated in [3] (see Section 2.2). Similarly, the numerical results for the circle for the 2-norm behave like k^β where β seems less than $-\frac{1}{2}$. If we had the result that $\|S\|_{L^2}$ behaved like $k^{-\frac{2}{3}}$ then this would also coincide with results from Section 2.2. However, we do not have this, but instead the results indicate that $\|S\|_{L^2}$ for a circle is behaving like k to a power less than what we had for an ellipse. This is expected and wanted if we are to have comparable results to that in [3].

Thus, assuming that the norm of our operator A is dominated by the term containing the single layer potential S our results give further evidence that for an ellipse $\|A\|$ behaves of the order $k^{\frac{1}{2}}$ and for a circle $\|A\|$ behaves of the order $k^{\frac{1}{3}}$.

The methodology used in this project also provides a crucial step in investigating properties of the operator A . Programming faster code and looking at more u for the 2-norm may give rise to a larger lower bound. Therefore, making the judgements on where $\|S\|_{L^2}$ lies in the region between the upper and lower bound less susceptible to error. Also, by looking at larger k for the circle the behaviour of the 2-norm may give stronger evidence of $\|S\|_{L^2}$ behaving like $k^{-\frac{2}{3}}$. This project can now be used as a tool and reference to enable A to be investigated even further and in more detail.

10 Future Work

There are three areas that would have been good to look into. These are the *lower norm*, further research into the two norm and looking at many more complicated convex shapes with smooth boundaries.

10.1 Lower Norms

We say that A is bounded below if $\exists M > 0$ such that,

$$\|Ax\| \geq M, \forall x \in X, \text{ with } \|x\| = 1$$

or

$$\|Ax\| \geq M\|x\| \forall x \in X.$$

The largest M is called the *lower norm* of A , and is denoted $|A|$. We can also write,

$$|A| = \inf_{\|x\|=1} \|Ax\|$$

or

$$|A| = \inf_{x \neq 0} \frac{\|Ax\|}{\|x\|}, \quad M \leq \|Ax\| \leq C \text{ if } \|x\| = 1 \text{ where } M \text{ and } C \text{ are constants.}$$

It is known that

$$|A| = \frac{1}{\|A^{-1}\|}$$

These lower norms are useful when looking at properties of the sound soft wave scattering problem. In this project we looked at $\|A\|$, studying the lower norm $|A|$ would allow us to investigate $\|A^{-1}\|$ as well. With the condition of the wave scattering problem bounded by $\|A\| \cdot \|A^{-1}\|$, this would then allow conclusions to be made about the condition number of A .

10.2 Further Research into the Two Norm

With more time and faster code it would be possible to gain a better lower bound on the two norm. Therefore, allowing better conclusions to be made on the norm $\|S\|_{L^2}$, which would give comparisons to the results from [3] to be made with much more assurity. Improving the upper bound as well would enable the region in which the 2-norm can lie to be further reduced. The

smaller the region then results about the 2-norm can be said with greater detail.

10.3 Looking at the Operator A

In this project we have only been looking at the operator S . By looking at all of the operator A we could make direct comparisons with the results provided in [3]. However, our conclusions for S correspond to similar conclusion that can be made for A .

References

- [1] Simon N. Chandler-Wilde and Peter Monk, Wave-Number-Explicit Bounds in Time-Harmonic Scattering (submitted for publication)
- [2] Mark Webber, The Point Source Method in Inverse Acoustic Scattering, MSc Dissertation, The University of Reading 2004
- [3] V. Dominguez, I.G. Graham and V.P. Smyshlyaev, A hybrid numerical-asymptotic boundary integral method for high-frequency acoustic scattering, Bath Institute For Complex Systems Preprint 1/2006
- [4] Edited by Milton Abramowitz and Irene A. Stegun, Handbook of Mathematical Functions With Formulas, Graphs and Mathematical Tables, Issued June 1964, Fourth Printing, December 1965, with corrections (page 11)
- [5] R. Lasser, Introduction to Fourier Series, Marcel Dekker, New York, 1996
- [6] Burden and Faires, Numerical Differentiation and Integration, Sixth Edition (Ch. 4)
- [7] D. Colton, R. Kress, Integral Equation Methods in Scattering Theory, Wiley, New York 1983
- [8] Stephen Arden, A Collocation Method for High Frequency Scattering By Convex Polygons, MSc Dissertation, The University of Reading 2005
- [9] Kendall E. Atkinson, The Numerical Solution of Integral Equations of the Second Kind, Cambridge University Press